INTERNATIONAL JOURNAL FOR NUMERICAL METHODS IN FLUIDS, VOL. 21, 1201–1220 (1995)

IMPLEMENTATION OF SOME HIGHER-ORDER CONVECTION SCHEMES ON NON-UNIFORM GRIDS

YUGUO LI

Division of Building, Construction and Engineering, CSIRO, Highett, Vic 3190, Australia

AND

LISA BALDACCHINO

Department of Mechanical Engineering, University of Melbourne, Parkville, Vic 3052, Australia

SUMMARY

A generalized formulation is applied to implement the quadratic upstream interpolation (QUICK) scheme, the second-order upwind (SOU) scheme and the second-order hybrid scheme (SHYBRID) on non-uniform grids. The implementation method is simple. The accuracy and efficiency of these higher-order schemes on non-uniform grids are assessed. Three well-known bench mark convection–diffusion problems and a fluid flow problem are revisited using non-uniform grids. These are: (1) transport of a scalar tracer by a uniform velocity field; (2) heat transport in a recirculating flow; (3) two-dimensional non-linear Burgers equations; and (4) a two-dimensional incompressible Navier–Stokes flow which is similar to the classical lid-driven cavity flow. The known exact solutions of the last three problems make it possible to thoroughly evaluate accuracies of various uniform and non-uniform grids. Higher accuracy is obtained for fewer grid points on non-uniform grids. The order of accuracy of the examined schemes is maintained for some tested problems if the distribution of non-uniform grid points is properly chosen.

KEY WORDS: higher-order schemes; non-uniform grids; discretization accuracy; finite-volume method

1. INTRODUCTION

Balancing accuracy and efficiency concerns in applying computational fluid dynamics (CFD) to industry has become the focus of many studies. One of the very important factors affecting prediction accuracy is the choice of discretisation schemes for the first-derivative convection schemes. The first-order upwind schemes (FOU) and the hybrid scheme as described by Spalding[1] were mostly used to avoid 'wiggles' introduced by the central difference (CD) scheme when the local cell Peclet number is larger than some critical value. However, these two schemes introduce excessive so-called numerical diffusion (dissipation), which exceeds actual physical diffusion if resolution is not sufficient. A number of higher-order upwind (weighted) schemes have been introduced, e.g. second-order upwind (SOU),[2] quadratic-upstream interpolation for convective kinematics (QUICK)[3], second-order hybrid scheme (SHYBRID),[17,12] and the fifth-order upwind scheme.[4] These schemes have been implemented, evaluated and applied in a number of applications.[5–7] Most of these studies on Cartesian grids used only uniform grids.

Non-uniform grids (using a finer grid in regions where high gradients of the flow quantity are involved) can reach a compromise between accuracy and efficiency. Extension of these schemes to non-uniform Cartesian grids is conceptually easy. However, the coefficients can be rather complex.

CCC 0271–2091/95/121201–20

Received 30 September 1994
Revised 5 May 1995

Different forms of the schemes on non-uniform grids can be found in Reference 8 for QUICK and Reference 9 for SOU and QUICK. Recently, Arampatzis and Assimacopoulos[10] developed a non-uniform grid version of QUICK based on three-dimensional quadratic interpolation functions in which the transverse curvature terms are maintained. The relative accuracy and efficiency of the numerical schemes vary among different test problems studied by different authors.[11] Thus, it is desirable to implement a number of higher-order schemes in a CFD code and to choose an 'optimum' one for a particular flow problem. The choice may be made by examining dominant flow features of the problem or by experience. Li and Rudman[12] presented a generalized formulation for the four-point discretisation schemes on non-uniform grids. The CD, QUICK, SOU and SHYBRID fall within this formulation. This facilitates an easy implementation of various schemes in a computer code. The transverse curvature terms were not included in the formulation. The formulation will be further examined and applied in the present work. It should be mentioned that if the locations with high gradients of the flow quantity are not known *a priori*, the non-uniform grids may not be directly used and an adaptive grid approach may be used. This is not discussed in this paper.

One difficulty in implementing higher-order schemes is that the coefficient matrix resulting from the finite difference equations may lose its diagonal dominance under conditions of highly convective flows. Thakur and Shyy[13] argued that the different implementation of the QUICK scheme may be responsible for inconsistent mixed findings in the literature as far as the stability of various implementation is concerned. Recent studies[13,14,6] showed that the deferred correction procedure of Khosla and Rubin[15] is the most robust and effective way. In this procedure, the standard first-order upwind (FOU) scheme is used to obtain the coefficients, which always results in a diagonally dominant matrix. The extra deferred correction term of the higher-order schemes is treated explicitly as a source term. This approach is adopted here.

There is a need to assess accuracy of higher-order schemes on non-uniform grids, but little work has been done in the literature. On non-uniform grids, many schemes may lose their order of accuracy as is observed through truncation error analysis of the Taylor series expansion[23]. Lack of detailed numerical experiments on this aspect gives rise to lack of confidence in using higher-order schemes on non-uniform grids. If variations of the dependent variables in the non-uniform grid regions or the aspect ratios are small, the loss of accuracy should be minimal. The higher-order schemes can also be implemented in a computational space with uniform grids which is transformed from a physical space. However, the influence of grid sizes on the accuracy is again introduced by the discretized metric coefficients. It should be mentioned that some other schemes such as Hermitian methods and compact methods (see review Chapter 4 in Reference 16) can maintain higher-order accuracy on non-uniform grids, but additional equations are needed to solve the first and higher derivatives. These schemes are not investigated in the present work. Another important aspect of higher-order schemes is the treatment of near-boundary points where higher-order schemes cannot be generally applied, since extra grid points outside the computational domain are required if the upwind direction is inward from the boundary. The first-order upwind scheme (FOU) is often used for the near-boundary points if the four-point schemes are used. Theoretically, the application of FOU reduces the accuracy of the higher-order scheme in the interior domain. Numerical experiments[13,12] show this approach can also give accurate results. However, some of the present results for a fluid flow problem are not promising. When non-uniform grids are used, the situation may be improved by using finer grids near the boundary, and this indeed is the conventional practice which resolves the thin regions of large gradients such as boundary layers adjacent to solid boundaries.

The objective of this study is two-fold.

(i) To implement three higher-order schemes QUICK, SOU and SHYBRID by using the generalised form proposed by Li and Rudman[12] for convection-dominated transport equations and incompressible Navier–Stokes flows.

(ii) To assess accuracy and efficiency of higher-order schemes on non-uniform Cartesian grids.

Four test cases are selected and investigated on various grids. These are: (1) transport of a scalar tracer by a uniform velocity field; (2) heat transport in a recirculating flow with exact equation given by Beier *et al.*[7] (3) two-dimensional non-linear Burgers equations with exact solutions given by Fletcher[21] and (4) a two-dimensional incompressible Navier–Stokes flow which is similar to the classical lid-driven cavity flow with exact solution given by Thakur and Shyy.[13] The schemes discussed in this paper deal only with incompressible flows, though an extension to compressible flows is not too difficult, e.g. by using a FCT flux limiter.[12]

2. GENERALIZED FORM OF FOUR HIGHER-ORDER SCHEMES

The generalized form was proposed by Li and Rudman.[12] For completeness, it is reviewed as follows. In Figure 1, the grid-related sizes $\delta_{iw}(i = 1, 2 \text{ and } 3)$ take different meanings when the velocity at the local face changes its direction. When $u_w > 0$, the variable at the west face, ϕ_w, can be approximated by different schemes. It is easy to show for CD that

$$\phi_w = \frac{\delta_{2w}}{\delta_{1w} + \delta_{2w}}\phi_W + \frac{\delta_{1w}}{\delta_{1w} + \delta_{2w}}\phi_P. \tag{1}$$

In SOU, ϕ_w is extrapolated from ϕ_W and ϕ_{WW}.

$$\phi_w = \frac{\delta_{3w}}{\delta_{3w} - \delta_{1w}}\phi_W - \frac{\delta_{1w}}{\delta_{3w} - \delta_{1w}}\phi_{WW}. \tag{2}$$

After some algebraic manipulation, equation (2) becomes

$$\phi_w = \frac{\delta_{2w}}{\delta_{1w} + \delta_{2w}}\phi_W + \frac{\delta_{1w}}{\delta_{1w} + \delta_{2w}}\phi_P - \frac{\delta_{1w}}{\delta_{1w} + \delta_{2w}}\left(\phi_P - \frac{\delta_{2w} + \delta_{3w}}{\delta_{3w} - \delta_{1w}}\phi_W + \frac{\delta_{1w} + \delta_{2w}}{\delta_{3w} - \delta_{1w}}\phi_{WW}\right). \tag{3}$$

QUICK uses a second-degree polynomial for calculating ϕ_w:

$$\phi_w = a_0 + a_1(x - x_P) + a_2(x - x_P)(x - x_W). \tag{4}$$

We have at $x = x_P$, $\phi_w = \phi_P$; at $x = x_W$, $\phi_w = \phi_W$; at $x = x_{WW}$, $\phi_w = \phi_{WW}$; thus a_0, a_1 and a_2 in (4) can be determined, giving

$$\phi_w = \phi_P + \frac{\phi_W - \phi_P}{x_W - x_P}(x_w - x_P) + \left[\frac{\phi_{WW} - \phi_P}{x_{WW} - x_P} - \frac{\phi_W - \phi_P}{x_W - x_P}\right]\frac{(x_w - x_P)(x_w - x_W)}{x_{WW} - x_W}. \tag{5}$$

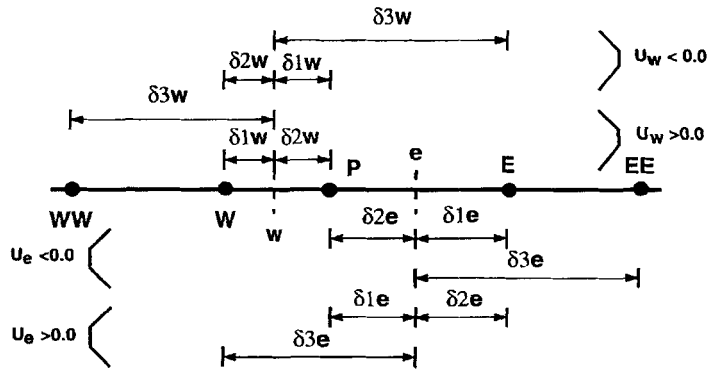

Figure 1. Grid system with grid related parameters in the x-direction

In terms of δ_i we obtain,

$$\phi_w = \phi_P + \frac{\delta_{2w}}{\delta_{1w}+\delta_{2w}}(\phi_W - \phi_P) + \frac{\delta_{1w}\delta_{2w}}{\delta_{3w}-\delta_{1w}}\left[\frac{\phi_W - \phi_P}{\delta_{1w}+\delta_{2w}} - \frac{\phi_{WW} - \phi_P}{\delta_{2w}+\delta_{3w}}\right], \tag{6}$$

i.e.

$$\begin{aligned}\phi_w = {} & \frac{\delta_{2w}}{\delta_{1w}+\delta_{2w}}\phi_W + \frac{\delta_{1w}}{\delta_{1w}+\delta_{2w}}\phi_P - \frac{\delta_{1w}\delta_{2w}}{(\delta_{1w}+\delta_{2w})(\delta_{2w}+\delta_{3w})} \\ & \times \left(\phi_P - \frac{\delta_{2w}+\delta_{3w}}{\delta_{3w}-\delta_{1w}}\phi_W + \frac{\delta_{1w}+\delta_{2w}}{\delta_{3w}-\delta_{1w}}\phi_{WW}\right).\end{aligned} \tag{7}$$

Equations (1), (3) and (7) can be expressed in the following generalized form, if $u_w > 0$,

$$\phi_w = \alpha_{2w}\phi_W + \alpha_{1w}\phi_P - q_w(\phi_P - \beta_{2w}\phi_W + \beta_{1w}\phi_{WW}). \tag{8}$$

The geometrical parameters are defined as

$$\begin{aligned}\alpha_{1w} &= \frac{\delta_{1w}}{\delta_{1w}+\delta_{2w}}, \beta_{1w} = \frac{\delta_{1w}+\delta_{2w}}{\delta_{3w}-\delta_{1w}}, \\ \alpha_{2w} &= \frac{\delta_{2w}}{\delta_{1w}+\delta_{2w}}, \beta_{2w} = \frac{\delta_{2w}+\delta_{3w}}{\delta_{3w}-\delta_{1w}}.\end{aligned} \tag{9}$$

The scheme parameters q_w take the appropriate forms for different schemes. For CD, $q_w = 0$; for SOU, $q_w = \alpha_{1w}$; and for QUICK,

$$q_w = \frac{\delta_{2w}}{\delta_{2w}+\delta_{3w}}\alpha_{1w}. \tag{10}$$

It can be easily derived, if $u_w < 0$, that

$$\phi_w = \alpha_{1w}\phi_W + \alpha_{2w}\phi_P - q_w(\phi_W - \beta_{2w}\phi_P + \beta_{1w}\phi_E). \tag{11}$$

It should be noted again that in Figure 1, δ_{iw}s represent different grid-related sizes when the face velocity reverses.

Equations (8) and (11) can be conventionally summarized as

$$\begin{aligned}F_w\phi_w = {} & (\alpha_{2w}\phi_W + \alpha_{1w}\phi_P - q_w(\phi_P - \beta_{2w}\phi_W + \beta_{1w}\phi_{WW}))F_w^+ \\ & + (\alpha_{1w}\phi_W + \alpha_{2w}\phi_P - q_w(\phi_W - \beta_{2w}\phi_P + \beta_{1w}\phi_E))F_w^-,\end{aligned} \tag{12}$$

where $F_w = \rho u_w A_w$ is the mass flow rate across the face w of the control volume and $F_w\phi_w$ is the net convection flux. A_w is the area of face w and ρ the density. The upwind mass flow rates F_w^+ and F_w^- over face w are defined as

$$F_w^+ = \frac{F_w + |F_w|}{2}, \qquad F_w^- = \frac{F_w - |F_w|}{2}. \tag{13}$$

For the east face,

$$\begin{aligned}F_e\phi_e = {} & (\alpha_{1e}\phi_E + \alpha_{2e}\phi_P - q_e(\phi_E - \beta_{2e}\phi_P + \beta_{1e}\phi_W))F_e^+ \\ & + (\alpha_{2e}\phi_E + \alpha_{1e}\phi_P - q_e(\phi_P - \beta_{2e}\phi_E + \beta_{1e}\phi_{EE}))F_e^-.\end{aligned}$$

Definitions of grid size parameters δ_{ie} can be found in Figure 1. Geometrical parameters α_{ie} and β_{ie}, and the scheme parameter q_e take a similar form as those in (9) and (12).

The second-order hybrid scheme (SHYBRID) can be obtained by examining the coefficients of the resulting discrete equation without deferred correction, using the generalized form (12) and (14)[12]. The scheme parameter q_f (f = e, w, n, s, h and l) is chosen so that the six neighbour-node coefficients are maintained positive.

If the local Peclet number $Pe_w = 0$, $q_w = 0$; if $Pe_w \neq 0$, then

$$q_w = \max\left[0, \alpha_{1w} - \frac{1}{|Pe_{rme}|}\right]. \tag{15}$$

The SHYBRID scheme is considered to reflect more closely the 'transportive' property of the partial differential equation than CD, QUICK or SOU. The value of the scheme parameter q_f is not fixed and is adjusted during the solution according to the magnitude of the local Peclet number. When the transport is diffusion-dominated, q_f is small ($< 1/\alpha_{1f}$), and SHYBRID is effectively the CD scheme. As q_f increases, the influence of the downstream nodes is reduced by taking into account the upwind nodes. When $Pe_f = (\delta_{2f}/\delta_{3f} + 1)/\alpha_{1f}$, SHYBRID is equivalent to QUICK. When q_f is very large or infinity, SHYBRID becomes the SOU scheme.

3. IMPLEMENTATION FOR CONVECTION-DIFFUSION PROCESS

In the first three test problems presented later, the two-dimensional transport equations are solved and they have the general form:

$$\frac{\partial \phi}{\partial t} + u\frac{\partial \phi}{\partial x} + v\frac{\partial \phi}{\partial y} = \gamma_\phi\left(\frac{\partial^2 \phi}{\partial x^2} + \frac{\partial^2 \phi}{\partial y^2}\right), \tag{16}$$

where u and v are the velocity components in the x and y directions respectively and γ_ϕ is the diffusion coefficient for the dependent variable ϕ. Equation (16) can be rewritten as

$$\frac{\partial \phi}{\partial t} + \frac{\partial (u\phi)}{\partial x} + \frac{\partial (v\phi)}{\partial y} = \gamma_\phi\left(\frac{\partial^2 \phi}{\partial x^2} + \frac{\partial^2 \phi}{\partial y^2}\right) + \phi\left(\frac{\partial u}{\partial x} + \frac{\partial v}{\partial y}\right). \tag{17}$$

For the first and second problems, $\nabla \cdot \mathbf{V} = \partial u/\partial x + \partial v/\partial y = 0$ and for the third problem, in which the two-dimensional Burgers equations are considered, the ϕ in (16) and (17) represents either u or v, and $\nabla \cdot \mathbf{V} \neq 0$.

The finite volume method is used to solve (17) with the appropriate boundary conditions, which will

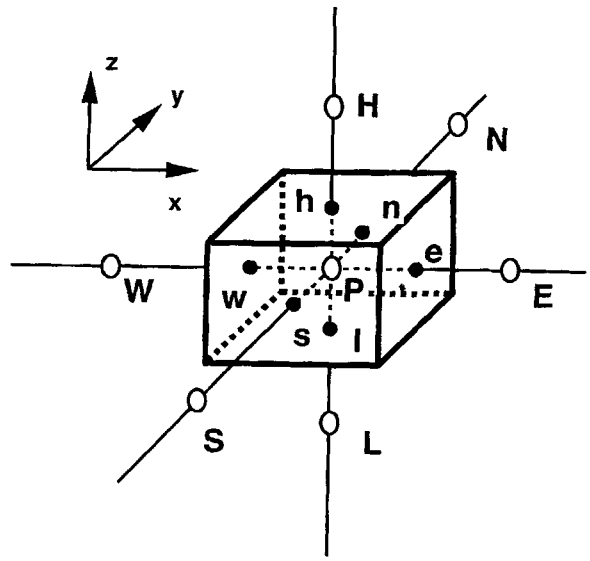

Figure 2. A control volume P with six surfaces (e, w, n, s, h and l) and six neighbouring node points (E, W, N, S, H, and L)

be specified in each test problem. It involves integrating locally over a finite control volume for time step Δt. Using the divergence theorem, we obtain the following discretized equation:

$$\frac{\phi_P - \phi_P^0}{\Delta t} V_P + J_e - J_w + J_n - J_s = \phi_P(u_e - u_w)A_e + \phi_P(v_n - v_s)A_n, \tag{18}$$

where A_f represents again the areas of the cell face f (f = e, w, n or s), and V_P is the cell volume. In the two-dimensional case in Figure 2, $A_e = y_n - y_s$, $A_n = x_e - x_w$ and $V_P = (x_e - x_w)(y_n - y_s)$. The superscript ^{0} represents the value at the previous time step, and J_f the total flux of ϕ across face f. For example,

$$J_e = \left[(u\phi)_e - \gamma_\phi\left(\frac{\partial\phi}{\partial x}\right)_e\right]A_e \equiv J_e^C + J_e^D, \tag{19}$$

where J_e^C is convective flux and J_e^D diffusive flux.

The CD scheme is used to discretize the diffusive terms, and we have

$$J_e^D = -\gamma_\phi\left(\frac{\partial\phi}{\partial x}\right)_e A_e = -\frac{\gamma_\phi}{x_E - x_P}(\phi_E - \phi_P)A_e. \tag{20}$$

For the convective flux J_e^C we have

$$J_e^C = [\phi u]_e A_e = F_e\phi_e. \tag{21}$$

The mass flow rate F_e is defined in the same way as previously, except the density is unity. The generalized form (14) is used to calculate the convective flux J_e^C, and to implement various higher-order schemes. For the first-order upwind scheme,

$$J_e^C = F_e^+\phi_P + F_e^-\phi_E. \tag{22}$$

At the near-boundary points, where sufficient nodes for higher order schemes are not available, FOU (equation (22)) is used.

In the test problems, only the steady-state solution is of interest, which is generally obtained by marching the transient solution with a constant time step. For the second test problem, when a stretching grid is used, the very small grid size near the boundary gives rise to a very small time step. Such a small time step results in an unacceptable convergence rate if a constant time step is used. Since only the steady-state solution is of interest, a pseudo-transient approach is used. The time step at each point is chosen based on a given Courant number $u\Delta t/\Delta x$ of 0·1 and diffusion number $\gamma_\phi\Delta t/\Delta x^2$ of 0·12. The two discretisation numbers are chosen so that the numerical scheme is stable. The method greatly improves the convergence to steady-state solution. Since the convergence is rapid, no attempt is directed at optimizing the solution parameters.

4. IMPLEMENTATION FOR INCOMPRESSIBLE FLOWS

While the explicit method is used for simulating convection-diffusion processes, a semi-implicit like method is used for incompressible flows. The above-mentioned higher-order schemes are implemented in a three-dimensional code, where the PISO (pressure-implicit with splitting of operators) algorithm[19] is used. PISO is found to perform better than SIMPLE[18] in the test problem. The governing equations are solved in a sequential manner. The velocity components are computed from the respective momentum equations. A pressure-correction equation, that is derived by manipulating continuity and momentum equations, is used to correct the pressure fields at the first stage and then velocity fields to satisfy the continuity. The corrected velocities are then used to calculate the coefficients of the pressure-correction equation at the second stage and to correct the pressure fields again. In the present

implementation of the PISO algorithm, the velocity fields are not corrected at the second stage as in the original PISO algorithm. The whole process is repeated until a convergent solution is obtained.

The general three-dimensional unsteady transport equation for a dependent variable ϕ in fluid flows can be written in Cartesian tensorial form,

$$\frac{\partial(\rho\phi)}{\partial t}+\frac{\partial(\rho u_j\phi)}{\partial x_j}=\frac{\partial}{\partial x_j}\left[\Gamma_\phi\left(\frac{\partial\phi}{\partial x_j}\right)\right]+S_\phi, \tag{23}$$

where ρ is the density, u_j the velocity vector with u, v and w components in the directions $x_1(x)$, $x_2(y)$ and $x_3(z)$ respectively, and S_ϕ the source term.

As done in (18), (23) is integrated locally over a finite control volume and the source term S_ϕ is linearized as $S_U+S_P\phi_P$. Using the divergence theorem, we obtain

$$\frac{\rho_P\phi_P-\rho\phi_P^0}{\Delta t}V_P+J_e-J_w+J_n-J_s+J_h-J_l=S_U+S_P\phi_P. \tag{24}$$

Again, J_f represents the total flux of the variable ϕ across face f (f = e, w, n, s, h or l), which contains two parts, J_f^C the convective flux and J_f^D the diffusive flux. The CD scheme is used to discretize the diffusive terms, for example,

$$J_e^D=-\left[\Gamma_\phi\frac{\partial\phi}{\partial x}\right]_e A_e=-D_e(\phi_E-\phi_P), \tag{25}$$

$$J_w^D=-\left[\Gamma_\phi\frac{\partial\phi}{\partial x}\right]_w A_w=-D_w(\phi_P-\phi_E), \tag{26}$$

where

$$D_e=\frac{\Gamma_{\phi,e}}{x_E-x_P}A_e, \tag{27}$$

$$D_w=\frac{\Gamma_{\phi,w}}{x_P-x_W}A_w. \tag{28}$$

If the generalized form of (12) and (14) is directly implemented in (24), after some algebraic manipulating, the following discretization equation is obtained:

$$a_P\phi_P=\sum_{nb=1}^{N}a_{nb}\phi_{nb}+C_0. \tag{29}$$

The number of neighbouring points N, the coefficients a_P, a_W, ..., and the source term c_0 of the discretization equation depend on the schemes used. As discussed in the introduction, the deferred correction procedure of Khosla and Rubin[15] is used in the present work. The standard first-order upwind scheme (FOU) is used to obtain the coefficient a_P and a_{nb}. Only six neighbouring points are involved implicitly. The extra deferred correction term of the higher-order scheme is included explicitly in the source term.

In this method, the net convective fluxes $F_e\phi_e$ and $F_w\phi_w$ in (11) and (14) are expressed as the sum of the first-order upwind fluxes (equation (22)) and the deferred correction fluxes, $(F\phi)_f^{dc}$.

$$F_e\phi_e=\phi_P F_e^+ + \phi_E F_e^- + (F\phi)_e^{dc}, \tag{30}$$

$$F_w\phi_w=\phi_W F_w^+ + \phi_P F_w^- + (F\phi)_w^{dc}, \tag{31}$$

where

$$(F\phi)_e^{dc} = (\alpha_{1e}\phi_E + (\alpha_{2e} - 1)\phi_P - q_e(\phi_E - \beta_{2e}\phi_P + \beta_{1e}\phi_W))F_e^+ + ((\alpha_{2e} - 1)\phi_E + \alpha_{1e}\phi_P - q_e(\phi_P - \beta_{2e}\phi_E + \beta_{1e}\phi_{EE}))F_e^-, \tag{32}$$

$$(F\phi)_w^{dc} = (\alpha_{1w}\phi_W + (\alpha_{2w} - 1)\phi_P - q_w(\phi_W - \beta_{2w}\phi_P + \beta_{1w}\phi_E))F_w^- + ((\alpha_{2w} - 1)\phi_W + \alpha_{1w}\phi_P - q_w(\phi_P - \beta_{2w}\phi_W + \beta_{1w}\phi_{WW}))F_w^+. \tag{33}$$

The resulting discretization equation is

$$a_P\phi_P = \sum_{nb=1}^{6} a_{nb}\phi_{nb} + c \tag{34}$$

where P = E, W, N, S, H or L and

$$c = S_U V_P + \frac{\rho_P V_P}{\Delta t}\phi_P^0 + c^{dc}. \tag{35}$$

The coefficients a_P and a_{nb} are obtained from the FOU discretization.[18] The extra deferred correction source term c^{dc} is

$$c^{dc} = -(F\phi)_e^{dc} + (F\phi)_w^{dc} - (F\phi)_n^{dc} + (F\phi)_s^{dc} - (F\phi)_h^{dc} + (F\phi)_l^{dc}. \tag{36}$$

As can be seen from above derivation, the present implementation method offers flexibility and ease for implementing various schemes. For CD, SOU, QUICK and SHYBRID schemes, the only difference is the scheme parameter q_f. It should be mentioned that if CD is used, $q_f = 0$, which indicates there is no need to evaluate β_{1f} and β_{2f} in (32) and (33).

5. RESULTS OF THE TEST CASE

5.1. Transport of a scalar tracer by a uniform velocity field

The problem involves convection and diffusion of a two-dimensional scalar field (16) with sharp gradients. The steady state velocity field is given by $u = 1$ and $v = 1$. The inlet boundary condition in the well-known Smith-Hutton problem[20] is imposed in the present calculation. The scalar displays a sharp but continuous change from 0 to 2 along the inlet. The boundary conditions can be summarized as

$$\phi = 1 + \tanh(20x + 10) \quad \text{at} \quad y = 0, -1 \leqslant x \leqslant 0,$$

$$\phi = 1 - \tanh(10) \quad \text{at} \quad x = -1, 0 \leqslant y \leqslant 1,$$

$$\frac{\partial\phi}{\partial n} = 0 \quad \text{at} \quad y = 1, -1 \leqslant x \leqslant 0,$$

$$\text{or} \quad x = 0, 0 \leqslant y \leqslant 1, \tag{37}$$

The maximum and minimum values of the solution are 2 and 0 respectively. No exact solution is available. However, the solutions on the finest grid using higher-order schemes can be used for comparison of accuracy. The main purpose here is to illustrate numerical diffusion of FOU and numerical dispersion of those higher-order schemes. The problem was run on a uniform and a non-uniform grid consisting of two uniform sections, and each of these were tested for four different grid

sizes (Figure 3). The numerical results are summarized in Table I. Eight examples of predicted scalar fields using FOU and QUICK are shown in Figure 4.

On the coarser grids, significant numerical diffusion is evident for FOU and numerical dispersion ('wiggles') for the higher-order schemes, as is reflected in the maximum and minimum values in Table I and scalar fields in Figure 4. As the grid is refined, inaccuracies due to numerical dispersion for higher-order schemes approach zero. At the grids 160 × 160 or 120 × 120, the overshoots have completely disappeared, and the undershoots are significantly reduced, particularly in the case of QUICK where the undershoots are now less than for other higher-order schemes. Due to a very high cell Peclet number, SHYBRID gives almost identical results to SOU. In the non-uniform grid solution, comparable (almost exact) levels of accuracy are achieved for fewer grid points than for corresponding

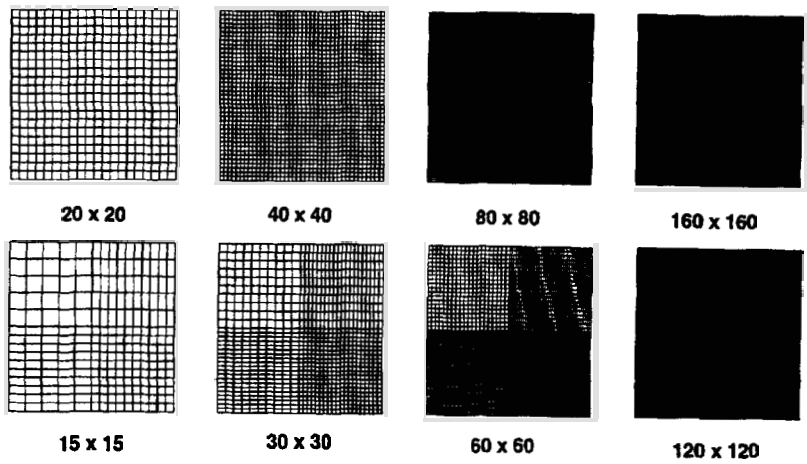

Figure 3. Four grid sizes of a uniform grid and a non-uniform grid used for the first test problem

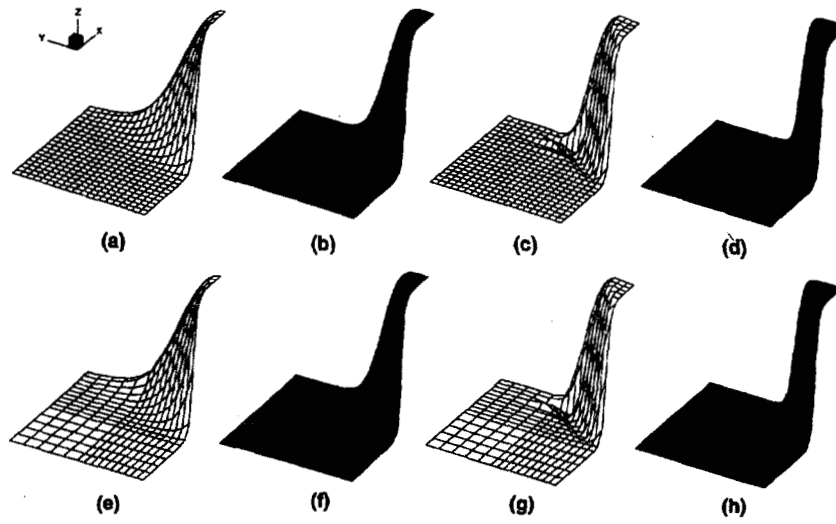

Figure 4. Predicted scalar fields using FOU (a, b, e, f) and QUICK (c, d, g, h) on 20 × 20 and 80 × 80 uniform grids (a, b, c, d) and 15 × 15 and 60 × 60 non-uniform grids (e, f, g, e, f, g, h)

Table I. Numerical results for transport of scalar tracer problem

Uniform Grid	20 × 20		40 × 40		80 × 80		160 × 160	
	Max	min	Max	min	Max	min	Max	min
FOU	1·9723	0	1·9995	0	2·0000	0	2·0000	0
SOU	2·0292	−0·0361	2·0209	−0·0267	2·0000	−0·0039	2·0000	−0·0015
QUICK	2·0326	−0·1725	2·0093	−0·0811	2·0000	−0·0024	2·0000	−0·0007
SHYBRID	2·0292	−0·0362	2·0209	−0·0267	2·000	−0·0039	2·0000	−0·0015

Non-Uniform Grid	15 × 15		30 × 30		60 × 60		120 × 120	
	Max	min	Max	min	Max	min	Max	min
FOU	1·9723	0	1·9995	0	2·0000	0	2·0000	0
SOU	2·0292	−0·0288	2·0209	−0·0251	2·0000	−0·0039	2·0000	−0·0016
QUICK	2·0326	−0·1765	2·0093	−0·0806	2·0000	−0·0024	2·0000	−0·0007
SHYBRID	2·0292	−0·0288	2·0209	−0·0251	2·0000	−0·0039	2·0000	−0·0016

uniform grids. This is an expected result; the problem is so designed that no variable-variation exists in the left half domain. Some blending or flux-limiting approaches can be used to suppress the oscillations ('wiggles') of these higher-order schemes (e.g. Reference 14). These are not investigated in the present work. In smooth incompressible flows, the higher-order schemes can still produce oscillation-free solutions as shown in the previous numerical experiences (e.g. Reference 6) and in the following three test problems.

5.2. *Heat transport in recirculating flow*

This excellent test problem with an exact solution was presented by Beier *et al.*,[7] who studied six convection discretisation schemes on uniform grids. The problem presents two important flow features in practical problems, namely recirculation and a temperature boundary layer. The problem involves a recirculating flow in a heated cavity (length l and height h) with the upper surface of the cavity being adiabatic, and the left and bottom surfaces being defined by a varying temperature profiles. The dependent variable ϕ in (16) is temperature. The flow is inviscid and the velocity field is obtained by the Schwartz–Christoffel transformation,

$$u = \frac{\pi}{2}\sinh\left(\frac{\pi x}{h}\right)\cos\left(\frac{\pi y}{h}\right), \tag{38}$$

$$v = \frac{\pi}{2}\cosh\left(\frac{\pi x}{h}\right)\sin\left(\frac{\pi y}{h}\right). \tag{39}$$

The exact solution of (16) is

$$\phi(r, s) = \mathrm{Re}[\exp(-Pe_\lambda s^2 + \Delta^2)erfc(\Delta)], \tag{40}$$

where Pe_λ is the half-plane Peclet number,

$$r = \frac{1}{2}\sqrt{\sqrt{\xi^2 + \eta^2} + \xi}, \tag{41}$$

$$s = \frac{1}{2}\sqrt{\sqrt{\xi^2 + \eta^2} - \xi}, \tag{42}$$

$$\Delta = \sqrt{(1 + Pe_\lambda)s} + ir. \tag{43}$$

The transformed coordinates ξ and η are

$$\xi = \frac{\lambda h}{2}\left[1 + \cosh\left(\frac{\pi x}{h}\right)\cos\left(\frac{\pi y}{h}\right)\right], \tag{44}$$

$$\eta = \frac{\lambda h}{2}\sinh\left(\frac{\pi x}{h}\right)\sin\left(\frac{\pi y}{h}\right), \tag{45}$$

where λ is the decay coefficient of the temperature profile along the left and bottom surface. A Peclet number Pe is defined with the maximum velocity in the x-direction in (38). The relationship between Pe and Pe_λ can be found in Reference 7. The test performed here uses a Peclet number of 200 in the same geometry as in Reference 7.

The boundary condition at $y/h = 1$ is $\partial\phi/\partial y = 0$ and those at other surfaces are defined in the original paper. For calculation purposes here, they are derived from the exact solution (40) applied at boundaries. The velocity field and exact solution of temperature ϕ for $Pe = 200$ are shown in Figure 5.

Three grid configurations each with four different grid sizes are used: a uniform grid, a non-uniform

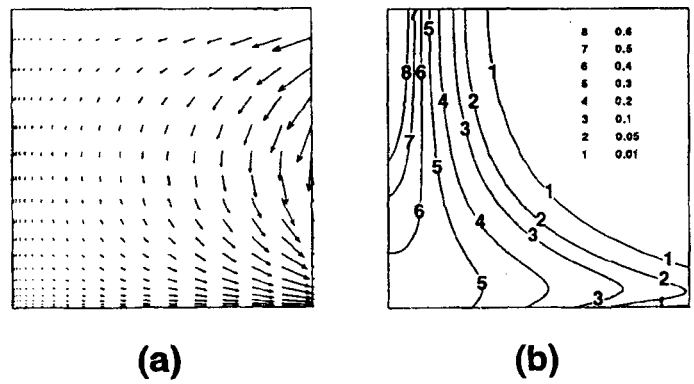

Figure 5. Velocity field (left) and exact solution of temperature field (right) for the second test problem

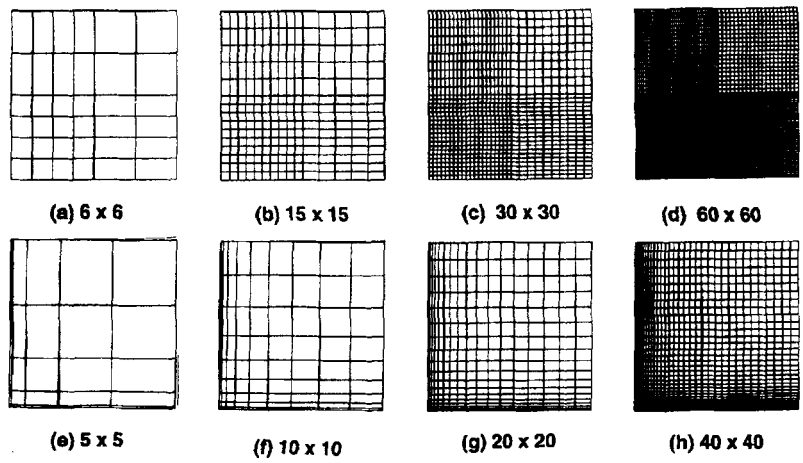

Figure 6. Four grid sizes of the two non-uniform grids for the second test problem

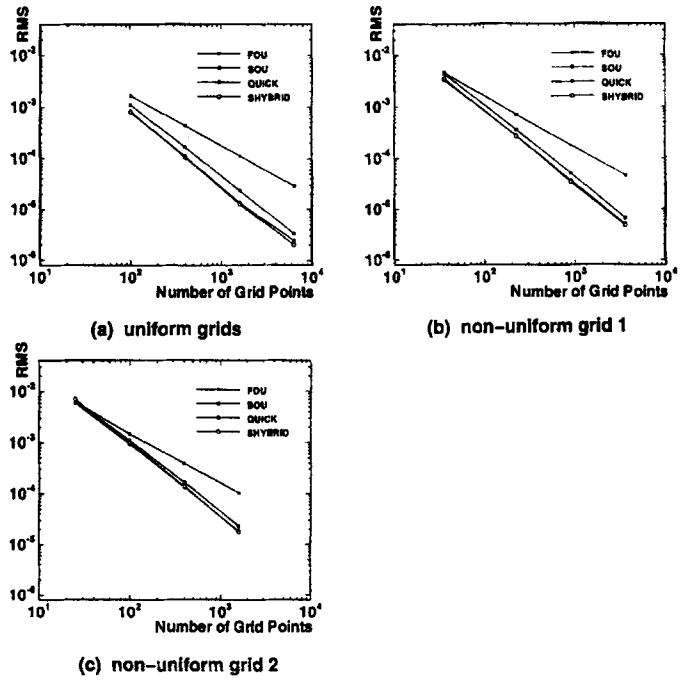

Figure 7. RMS plots for heat transport in recirculating flow problem

grid consisting of two uniform sections (non-uniform grid 1), and a stretched grid (non-uniform grid 2); see Figure 6 for the two non-uniform grids. The numerical results are summarised in Table II, where the root mean square (rms) error is presented. The results are also plotted in Figure 7 for each grid configuration.

The higher-order schemes are consistently superior to FOU. It is notable that higher-order schemes maintain higher than first order accuracy on all non-uniform grids studied here. However, when we plot rms error for each scheme separately (not shown) instead of for each grid configuration in Figure 7, it can be seen that QUICK and SHYBRID on stretched grids perform almost equally badly as with uniform grids, particularly on finer grids, suggesting some loss in order of accuracy, as is shown by Taylor series expansion. SOU displays significantly less accuracy than SHYBRID and QUICK, although it is notably superior to its first-order counterpart. The similarity between QUICK and SHYBRID is not surprising considering that the hybrid solution approaches QUICK at moderate Peclet numbers. However, it is also notable that SHYBRID does yield a better result to QUICK on the finest non-uniform grid 1. Due to the fact that SHYBRID represents the transportive property of the flow in a much closer way than QUICK, it is expected that SHYBRID will be superior to QUICK in more complex problems.

Due to stability and convergence considerations, it is necessary to use various time steps at different grid points for the stretched grids, and hence it is not possible to draw any significant conclusions from a comparison of CPU time between the stretched and the other grids. By comparing CPU times required for the first two grids, it can be seen that the non-uniform grid solutions are more efficient. For this problem, the flow is inviscid and no velocity boundary layer exists. The thermal boundary layers do not result in very severe gradients for the Peclet number of 200 used here. Even though the non-uniform grids give better solutions than uniform grids, when the grid is finer, this improvement is very small. This highlights the importance and difficulties of choosing a proper grid distribution.

Table II. Numerical results for recirculating flow in a heated cavity problem

Uniform Grid	10 × 10 RMS	10 × 10 CPU Time	20 × 20 RMS	20 × 20 CPU Time	40 × 40 RMS	40 × 40 CPU Time	80 × 80 RMS	80 × 80 CPU Time
FOU	1·6872E-3	0·98	4·4139E-4	5·00	1·1362E-4	54·26	2·9067E-5	690·44
SOU	1·1251E-3	0·90	1·6759E-4	5·32	2·3607E-5	56·63	3·3049E-6	750·27
QUICK	8·3990E-4	0·81	1·1056E-4	5·11	1·3519E-5	56·00	2·4017E-6	690·84
SHYBRID	8·2639E-4	0·75	1·0574E-4	5·55	1·2712E-5	58·09	1·9978E-6	732·37

Non-Uniform Grid	6 × 6 RMS	6 × 6 CPU Time	15 × 15 RMS	15 × 15 CPU Time	30 × 30 RMS	30 × 30 CPU Time	60 × 60 RMS	60 × 60 CPU Time
FOU	4·6424E-3	0·31	7·0498E-4	3·04	1·7835E-4	30·53	4·5834E-5	360·96
SOU	4·4345E-3	0·23	3·5842E-4	1·22	5·0426E-5	28·77	6·5918E-6	403·28
QUICK	3·3431E-3	0·23	2·7318E-4	2·43	3·6386E-5	33·09	4·9721E-6	395·56
SHYBRID	3·5343E-3	0·37	2·6832E-4	1·45	3·3836E-5	32·96	4·7323E-6	405·95

Non-Uniform Grid 2	5 × 5 RMS	5 × 5 CPU Time	10 × 10 RMS	10 × 10 CPU Time	20 × 20 RMS	20 × 20 CPU Time	40 × 40 RMS	40 × 40 CPU Time
FOU	6·2903E-3	0·22	1·4547E-3	0·91	3·8689E-4	7·26	1·0275E-4	88·77
SOU	6·4985E-3	0·27	1·0890E-3	0·77	1·6527E-4	7·85	2·2998E-5	93·86
QUICK	5·9227E-3	0·25	9·3392E-4	0·78	1·3296E-4	8·26	1·8016E-5	98·46
SHYBRID	6·99-5E-3	0·31	9·9663E-4	0·88	1·3697E-5	9·11	1·7680E-5	100·87

5.3. *Two-dimensional Burgers equations*

In the above two test problems, nonlinearities are not present. As a simplified form of the Navier–Stokes equations, the Burgers equations serve as a good model for non-linear flow problems. By using the Cole–Hopf transformation, Fletcher[21] constructed an interesting exact solution of the two-dimensional Burgers equations. In (16), ϕ represents u or v, and γ_ϕ represents viscosity ν, i.e.

$$\frac{\partial u}{\partial t} + u\frac{\partial u}{\partial x} + v\frac{\partial u}{\partial y} = \nu\left(\frac{\partial^2 u}{\partial x^2} + \frac{\partial^2 u}{\partial y^2}\right), \tag{46}$$

$$\frac{\partial v}{\partial t} + u\frac{\partial v}{\partial x} + v\frac{\partial v}{\partial y} = \nu\left(\frac{\partial^2 v}{\partial x^2} + \frac{\partial^2 v}{\partial y^2}\right), \tag{47}$$

The exact solution is

$$u = -\frac{2\nu[a_2 + a_4 y + \lambda a_5(e^{\lambda(x-x_0)} - e^{-\lambda(x-x_0)})\cos(\lambda y)]}{[a_1 + a_2 x + a_3 y + a_4 xy + a_5(e^{\lambda(x-x_0)} + e^{-\lambda(x-x_0)})\cos(\lambda y)]}, \tag{48}$$

$$u = -\frac{2\nu[a_3 + a_4 y - \lambda a_5(e^{\lambda(x-x_0)} + e^{-\lambda(x-x_0)})\sin(\lambda y)]}{[a_1 + a_2 x + a_3 y + a_4 xy + a_5(e^{\lambda(x-x_0)} + e^{-\lambda(x-x_0)})\cos(\lambda y)]}. \tag{49}$$

In the test case here, we use an exact solution with a severe internal gradient (Figure 8), which is generated by the following parameter values,

$$a_1 = a_2 = 1{\cdot}3 \times 10^{13}, \quad a_3 = a_4 = 0, \quad a_5 = 1{\cdot}0, \quad \lambda = 25, \quad x_0 = 1, \quad \nu = 0{\cdot}04. \tag{50}$$

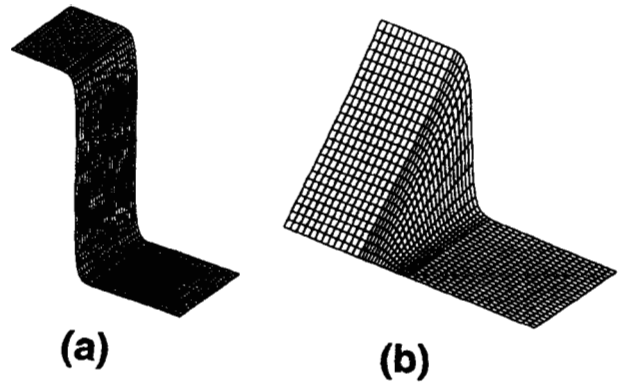

Figure 8. An exact solution for u and v on a non-uniform grid with an internal gradient

Five grid configurations are used, each with four grid sizes, see Figure 9. More than one type of non-uniform grid is used in order to assess the influence of grid smoothness on the solution accuracy and efficiency. A constant time step is used for all the steady-state solutions. The relative accuracy and CPU time spent of each scheme for all the grids are summarised in Table III, and the rms errors of u-component for each scheme are also plotted in Figure 10.

QUICK is almost consistently the most accurate and FOU is the least accurate, except for the coarsest grid. The nature of the solution renders it particularly appropriate for use with non-uniform grids. From Table III, it is clear that higher accuracy is maintained for fewer grid points on non-uniform grids, which also results in less CPU time. By plotting the error distribution of the u-solution on uniform and non-uniform grids (not shown), it is found as expected that grid refinement by use of

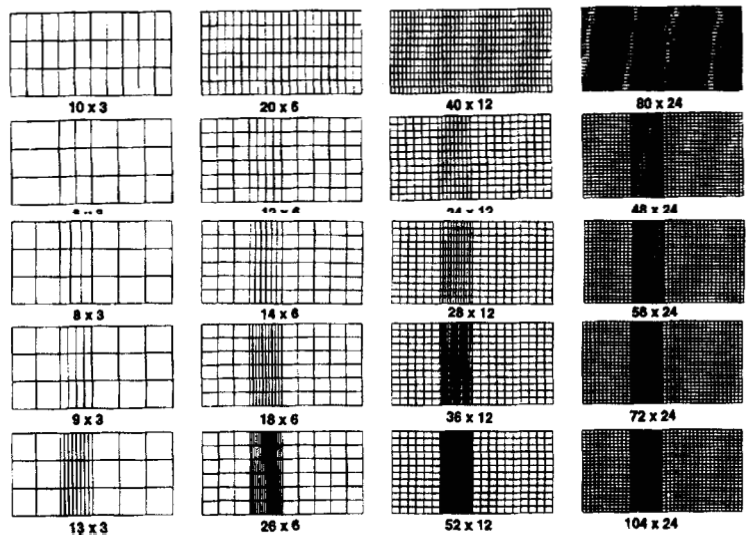

Figure 9. Four grid sizes of a uniform grid and four non-uniform grids used for the third test problem. The four non-uniform grids are referred as non-uniform grid 1, 2, 3, and 4 in the text, where the number represents the grid fineness in the refined region. The larger the number, the finer the grid in the refined region

Table III. Numerical results for the two-dimensional Burgers equations

Uniform Grid	10 × 3		20 × 6		40 × 12		80 × 24	
	RMS U	RMS V	RMS U	RMS V	RMS U	RMS V	RMS U	RMS V
FOU	6·771E-4	1·744E-3	1·577E-4	3·631E-4	5·211E-5	8·317E-5	1·439E-5	1·969E-5
SOU	6·108E-4	1·895E-3	1·122E-4	2·860E-4	2·855E-5	3·867E-5	6·116E-6	4·702E-6
QUICK	7·145E-4	1·921E-3	1·006E-4	2·863E-4	1·655E-5	3·781E-5	4·704E-6	4·524E-6
SHYBRID	7·569E-4	1·928E-3	1·247E-4	2·860E-4	1·964E-5	3·774E-5	4·958E-6	4·517E-6
Non-Uni Grid 1	6 × 3		12 × 6		24 × 12		48 × 24	
	RMS U	RMS V	RMS U	RMS V	RMS U	RMS V	RMS U	RMS V
FOU	1·146E-3	1·783E-3	2·707E-4	4·600E-4	8·779E-5	1·053E-4	2·374E-5	2·490E-5
SOU	1·032E-3	1·949E-3	1·912E-4	3·632E-4	4·722E-5	4·907E-5	9·198E-6	6·004E-6
QUICK	1·291E-3	1·981E-3	1·614E-4	3·661E-4	2·613E-5	4·805E-5	6·602E-5	5·755E-6
SHYBRID	1·333E-3	1·991E-3	2·138E-4	3·674E-4	3·171E-5	4·837E-5	7·085E-6	5·797E-6
Non-Uni Grid 2	8 × 3		14 × 6		28 × 12		56 × 24	
	RMS U	RMS V	RMS U	RMS V	RMS U	RMS V	RMS U	RMS V
FOU	1·067E-3	1·994E-3	2·499E-4	4·206E-4	6·692E-5	9·650E-5	1·778E-5	2·281E-5
SOU	9,975E-4	2·173E-3	1·620E-4	3·336E-4	2·832E-5	4·490E-5	6·567E-6	5·464E-6
QUICK	7·896E-4	2·201E-3	1·058E-4	3·331E-4	1·707E-4	4·406E-5	5·781E-6	5·271E-6
SHYBRID	7·182E-4	2·240E-3	1·177E-4	3·335E-4	1·963E-5	4·403E-5	5·901E-6	5·276E-6
Non-Uni Grid 3	9 × 3		18 × 6		36 × 12		72 × 24	
	RMS U	RMS V	RMS U	RMS V	RMS U	RMS V	RMS U	RMS V
FOU	6·373E-4	1·845E-3	1·758E-4	3·666E-4	4·379E-5	8/411E-5	1·188E-5	1·991E-5
SOU	5·515E-4	2·012E-3	8·956E-5	2·921E-4	1·569E-5	3·939E-5	5·095E-6	4·777E-6
QUICK	5·140E-4	2·040E-3	6·073E-5	2·901E-4	1·255E-5	3·845E-5	4·979E-6	4·597E-6
SHYBRID	5·300E-4	2·051E-3	6·378E-5	2·896E-4	1·311E-5	3·816E-5	5·024E-6	4·549E-6
Non-Uni Grid 4	13 × 3		26 × 6		52 × 12		104 × 24	
	RMS U	RMS V	RMS U	RMS V	RMS U	RMS V	RMS U	RMS V
FOU	4·763E-4	1·494E-3	1·001E-4	3·024E-4	2·531E-5	6·945E-5	7·442E-6	1·647E-5
SOU	3·605E-4	1·631E-3	3·746E-5	2·384E-4	1·002E-5	3·156E-5	4·247E-6	3·763E-6
QUICK	3·124E-4	1·651E-3	3·746E-5	2·384E-4	1·002E-5	3·156E-5	4·247E-6	3·763E-6
SHYBRID	3·035E-4	1·658E-3	3·777E-5	2·375E-4	1·023E-5	3·130E-5	4·245E-6	3·714E-6

non-uniform grids reduces the error in the refined region. The grid number in the y-direction is kept constant in each grid group. It can be seen in Table III that the v-rms error is slightly larger in the non-uniform grid 1 than the corresponding uniform grid (It should also be noted that u-rms error is also slightly larger), but gradually reduced, when the grid in the large-gradient region in the x-direction is refined. This may be due to the fact that u and v are strongly coupled.

In Figure 10, a downward shift of the rms profile as the grid in the larger-gradient region is refined, will indicate a gain in solution accuracy by the use of fewer grid points. For FOU, this is true at a larger number of grid points, but not true at a small number of grid points. But for the higher-order schemes QUICK and SHYBRID, this is true at a small number of grid points and not true at a large number of grid points. For SOU the results are different and complex. With a very large grid aspect ratio $(x_{i+1} - x_i)/(x_i - x_{i-1})$ of 0·0625 in non-uniform grid 4, the solution accuracy does not improve

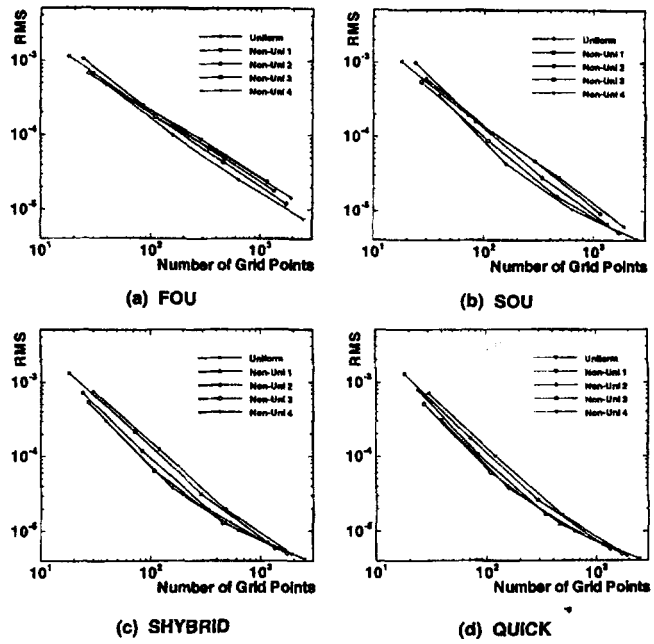

Figure 10. RMS plots for (a) FOU, (b) SOU, (c) SHYBRID and (d) QUICK schemes in computing u of the 2D Burgers equations

compared to non-uniform grid 3. At very large grid numbers tested, even a grid aspect ratio of 0·25 in non-uniform grid 2 does not give any better results for QUICK and SHYBRID. The importance of these results can be seen from the fact that in most engineering calculations, coarse grids are generally used. The results discussed above imply that non-uniform grid, together with higher-order schemes such as QUICK and SHYBRID, can be a useful approach. The advantages of using non-uniform grids with FOU and SOU are still present at a smaller number of grid points, but not superior to QUICK and SHYBRID. Overall, the use of non-uniform grids in this test problem is very successful and encouraging. The detailed analysis of the influence of grid aspect ratios can be expected to provide guidance for the behaviour of non-uniform grids applied to real fluid flows.

5.4. Lid-driven cavity like flow

This test flow problem, whose exact solution is known, was constructed by Shih *et al.*[22] to assess the effects of grid staggering. The flow with artificially designed body forces is qualitatively similar to the classical lid-driven cavity flow. The governing equations are

$$\frac{\partial u}{\partial x}+\frac{\partial v}{\partial y}=0, \tag{51}$$

$$\frac{\partial u}{\partial t}+u\frac{\partial u}{\partial x}+v\frac{\partial u}{\partial y}=v\left(\frac{\partial^2 u}{\partial x^2}+\frac{\partial^2 u}{\partial y^2}\right)-\frac{\partial p}{\partial x}, \tag{52}$$

$$\frac{\partial v}{\partial t}+u\frac{\partial v}{\partial x}+v\frac{\partial v}{\partial y}=v\left(\frac{\partial^2 v}{\partial x^2}+\frac{\partial^2 v}{\partial y^2}\right)-\frac{\partial p}{\partial y}-f, \tag{53}$$

where p is pressure and f the body force source term for v-equation. The expression for f and the solution pressure p is very lengthy and will not be repeated here. Details can be found in the original paper. The boundary conditions for u and v at the top surface ($y=1$) are $v=0$ and

$$u = 16(x^4 - 2x^3 + x^2) \tag{54}$$

and are of Dirichlet type zero at other surfaces. The advantage of these boundary conditions is that velocities at the two top corners are zero.

The exact solutions of u and v are

$$u = 8(x^4 - 2x^3 + x^2)(4y^3 - 2y), \tag{55}$$

$$v = -8(4x^3 - 6x^2 + 2x)(y^4 - y^2). \tag{56}$$

Shih *et al.*[22] obtained numerical solution only for $v=0{\cdot}1$, since a central difference scheme was used. In the present work, a solution is obtained for $v=0{\cdot}001$ for all the schemes tested. The exact solution is plotted in Figure 11.

Two grid configurations are used, a uniform grid and a non-uniform grid consisting two uniform sections in the y-direction. An example of a non-uniform grid 40 × 30 and solution by QUICK on that grid is shown in Figure 12. The solution rms errors for u, v and $\partial p/\partial y$ are summarised in Table IV.

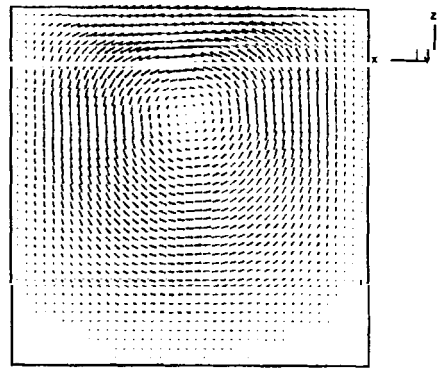

Figure 11. Exact solution of the lid-driven like flow, which is given by (55 and 56)

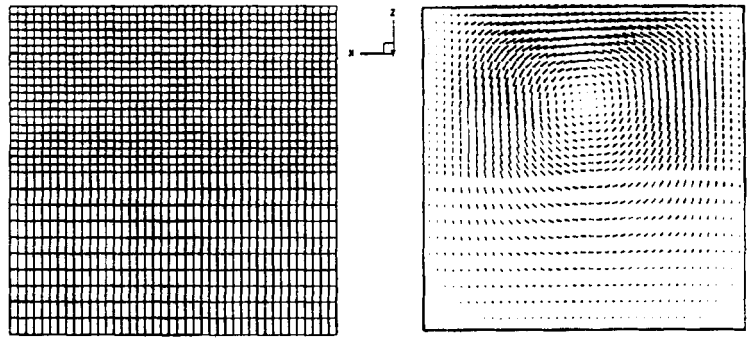

(a) (b)

Figure 12. (a) Non-uniform grid 40 × 30; and (b) velocity solution of the fourth test problem by the QUICK scheme on grid 40 × 30

Table IV. Numerical results for the lid-driven flows

Uniform Grid	FOU	QUICK	SOU	SHYBRID
		U-RMS		
20 × 20	4·3703E-2	3·0315E-2	3·3902E-2	3·0594E-2
40 × 40	2,1381E-2	1·3671E-2	1·2804E-2	1·4476E-2
80 × 80	1·4562E-2	9·9503E-3	9·7030E-3	1·0240E-2
		V-RMS		
20 × 20	5·5414E-2	3·2513E-2	5·0502E-2	4·0258E-2
40 × 40	2·9701E-2	1·2531E-2	1·3442E-2	1·2821E-2
80 × 80	1·7149E-2	8·9801E-3	8·8414E-3	9·2066E-3
		∂p/∂y-RMS		
20 × 20	4·7451E-2	4·4325D-2	5·7583E-2	4·6775E-2
40 × 40	2·8079E-2	2·4617E-2	2·1302E-2	2·7372E-2
80 × 80	2·2242E-2	2·0999E-2	2·0347E-2	2·1726E-2
Non-Uniform Grid	**FOU**	**QUICK**	**SOU**	**SHYBRID**
		U-RMS		
20 × 16	2·9948E-2	3·6796E-2	3·9165E-2	3·6935E-2
40 × 30	2·3163E-2	1·5942E-2	1·5276E-2	1·6664E-2
80 × 60	1·4867E-2	1·669E-2	1·0956E-2	1·1455E-2
		V-RMS		
20 × 16	6·0709E-2	3·8069E-2	5·5368E-2	4·5694E-2
40 × 30	3·2961E-2	1·5052E-2	1·6074E-2	1·5302E-2
80 × 60	1·8622E-2	1·0606E-2	1·0474E-2	1·0843E-2
		∂p/∂y-RMS		
20 × 16	5·3298E-2	5·2529E-2	6·0180E-2	5·2857E-2
40 × 30	3·0892E-2	2·9482E-2	2·6059E-2	3·2242E-2
80 × 60	2·3739E-2	2·4410E-2	2·3801E-2	2·5151E-2

Even though the use of higher-order schemes improves the solution accuracy, the higher-order accuracy of SOU, SHYBRID and QUICK is not maintained even on uniform grids. Calculation shows that the present implementation of higher-order schemes in the flow code is robust. The solution accuracy on non-uniform grids with higher-order schemes is better than that with FOU. It appears that QUICK and SOU predict better $\partial p/\partial y$ than SHYBRID. The results indicate the complexity of numerical prediction in a flow problem. The reason for loss of order of accuracy of higher-order schemes is unknown to the authors. It may be hypothesised that this is due to the use of FOU at near-boundary points. Application of FOU at near-boundary points in the second and third problems studied did not result in a great loss of order of accuracy. The reason that it happens in the flow problem here may be due to the elliptic behaviour of pressure. Further investigation will be carried out by using a consistent extrapolation method to define variables at external pseudo-nodes.

6. CONCLUSIONS

An easy implementation method has been presented for three higher-order schemes on non-uniform grids for both convection-diffusion and incompressible flow problems. The implementation method involves an application of a generalized scheme formulation. The schemes have been tested on various

uniform and non-uniform grid configurations for four problems, in which three have exact solutions for accuracy assessment. Overall, higher accuracy is obtained for fewer grid points on non-uniform grids. It is confirmed that the order of accuracy of the examined schemes can be maintained if the non-uniform grid points are properly chosen to be in small-variation regions of the dependent variables, and the grid size aspect ratio is small. The application of a first-order upwind scheme at near-wall points does not result in a great loss of order of accuracy for all the convection-diffusion problems, but seems to do so for flow problems, which requires further investigation.

ACKNOWLEDGEMENT

We thank Dr Angelo Delsante and Dr Jeff Symons for their encouragement and discussions. During the course of this study, Lisa Baldacchino worked as a vacation student at CSIRO.

NOMENCLATURE

a	coefficient in (34)
A	area of the face of the control volume
c	coefficient in (34)
C	correction factor of the anti-diffusive flux
D	diffusion-like term in (27) and (28)
F	mass flow rate across the face of the control volume
J	convective flux
p	pressure
Pe	Peclet number ($=F/D$)
q	scheme parameter used first in (4)
S_ϕ	source term in (23)
S_P, S_U	coefficients in the linearised for of source term S_ϕ
t	time
u_i	velocity components along x_i axes
u, v	velocity components along x and y axes, respectively
V	cell volume
x, y	axes of Cartesian coordinate system

Greek symbols

α, β	geometrical parameters defined in (9)
γ_ϕ	diffusion coefficient in (16)
Γ_ϕ	diffusion coefficient in (23)
δ	length associated with grid size, (defined in Figure 1)
ν	viscosity
ρ	fluid density
ϕ	dependent variable

Subscripts

e, w, n, s, h, l	east, west, north, south, high and low surfaces of control volume centre at node P

E, W, N, S	east, west, north and south nodes adjacent to node P
EE, WW, NN, SS	nodes 2 cells distant from P in east, west, north and south directions
P	nodal point to be considered

REFERENCES

1. D. B. Spalding, 'A novel finite difference formulation for differential expressions involving both first and second derivatives.' *Int. j numer. methods Eng.*, **4**, 551–559 (1972).
2. R. F. Warming and R. M. Beam, Upwind second-order difference schemes and applications in aerodynamic flows', *AIAA J.*, **14**, 1241–1249 (1976).
3. B. P. Leonard, 'A stable and accurate convective modelling procedure based on quadratic upstream interpolation'. *Computer Meth. Appl. Mech. Eng.*, **19**, 59–98 (1979).
4. M. M. Rai, 'Navier–Stokes simulations of blade-vortex interaction using high-order accurate upwind schemes', *AIAA Paper 87-0543*, 1987.
5. W. Shyy, 'A study of finite difference approximations to steady-state convection dominated flow problems', *J. Comput. Phys.*, **57**, 415–437 (1985).
6. P. Tamamidis and D. N. Assanis, 'Three-dimensional incompressible flow calculations with alternative discretization schemes', *Numer. Heat Transfer*, B **24**, 57–76 (1993).
7. R. A. Beier, J. de Ris and H. R. Baum, 'Accuracy of finite-difference methods in recirculating flows', *Numer. Heat Transfer*, **6**, 283–302 (1983).
8. C. J. Freitas, R. L. Street, A. N. Findikakis and J. R. Koseff, 'Numerical simulation of three-dimensional flow in a cavity,' *Int. j. numer. meth. fluids*, **5**, 561–575 (1985).
9. M. A. R. Sharif and A. Busnaina, 'Assessment of finite difference approximation for the advection terms in the simulation of practical flow problems', *J. Comput. Phys.*, **74**, 143–176 (1988).
10. G. Arampatzis and D. Assimacopoulos, 'Treatment of numerical diffusion in strong convection flows', *Int. j. numer. meth. fluids*, **18**, 313–331 (1994).
11. S. V. Patankar, 'Recent developments in computational heat transfer', *J. Heat Transfer*, **110**, 1037–1045 (1988).
12. Y. Li and M. Rudman, 'Assessment of higher-order upwind schemes incorporating FCT for linear and nonlinear convection-dominated problems', *Numer. Heat Transfer*, B **27**, 1–21 (1995).
13. S. Thakur and W. Shyy, 'Some implementation issues of convection schemes for finite-volume formulations', *Numer. Heat Transfer*, B **24**, 31–55 (1993).
14. M. S. Darwish, 'A new high-resolution scheme based on the normalized variable formulation', *Numer. Heat Transfer*, B **24**, 353–371 (1993).
15. P. K. Khosla and S. G. Rubin, 'A diagonally dominant second-order accurate implicit scheme', *Computers Fluids*, **2**, 207–209 (1974).
16. C. Hirsch, *Numerical Computation of Internal and External Flows*, Vol. 1, John Wiley Sons, New York, 1988.
17. Y. Matsuo, J. J. Yee, T. Kurabuchi and M. Kamata, 'Highly accurate and non-oscillatory finite-difference approximation method for convection diffusion equations', in *Int. Symp. on Room Air Convection and Ventilation Effectiveness*, University of Tokyo, 358–365, 1992.
18. S. V. Patankar, *Numerical Heat Transfer and Fluid Flow*, Hemisphere, Washington DC, 1980.
19. R. I. Issa, A. D. Gosman and A. P. Watkins, 'The computation of compressible and incompressible recirculating flows by a non-iterative scheme', *J. Comput. Phys.*, **62**, 66–72 (1986).
20. R. M. Smith and A. G. Hutton, 'The numerical treatment of advection: a performance comparison of current methods', *Numer. Heat Transfer*, **5**, 439–461 (1982).
21. C. A. J. Fletcher, 'Generating exact solutions for the two-dimensional Burgers equations', *Int. j. numer. meth. fluids*, **3**, 213–216 (1983).
22. T. M. Shih, C. H. Tan and B. C. Hwang, 'Effects of grid staggering on numerical schemes', *Int. j. numer. meth. fluids*, **9**, 193–212 (1989).
23. J. D. Hoffman, 'Relationship between the truncation errors of centered finite difference approximation on uniform and non-uniform meshes', *J. Comput. Phys.*, **46**, 469–477 (1982).